

Study of $\pi^-p \rightarrow \eta n$ at low energies in a chiral constituent quark model

Xian-Hui Zhong¹ and Qiang Zhao^{1,2}

1) *Institute of High Energy Physics, Chinese Academy of Sciences, Beijing 100049, P.R. China* and

2) *Department of Physics, University of Surrey, Guildford, GU2 7XH, United Kingdom*

Jun He and Bijan Saghai

*Laboratoire de recherche sur les lois fondamentales de l'Univers,
DAPNIA/SPhN, CEA/Saclay, 91191 Gif-sur-Yvette, France*

A chiral quark model approach is extended to the study of the πN scattering at low energies. The process of $\pi^-p \rightarrow \eta n$ near threshold is investigated. The model is successful in describing the differential cross sections and total cross section near the η production threshold. The roles of the resonances in $n \leq 2$ shells are clarified. Near threshold, the $S_{11}(1535)$ dominates the reactions, while the interferences from the $S_{11}(1650)$ turn out to be destructive around $W \lesssim 1.6$ GeV. The $D_{13}(1520)$ is crucial to give correct shapes of the differential cross sections. The nucleon pole term contributions are significant. The $P_{11}(1710)$ plays an important role around the c.m. energy $W = 1.7$ GeV, it is crucial to produce an enhancement in the region of $W > 1.6$ GeV as suggested by the data for total cross section. The t -channel is negligible in the reactions.

PACS numbers: 25.80.Hp, 11.80.Et, 13.60.Le, 12.39.Jh

I. INTRODUCTION

The $\pi^-p \rightarrow \eta n$ reaction at low energies is an interesting topic in nuclear physics. This reaction can provide a good probe into the structure of some low-lying resonances, such as $S_{11}(1535)$, of which the property still bares a lot of controversies. In the naive quark model, it is classified as the lowest $L = 1$ orbital excited state with $J^P = 1/2^-$. Recently, it is argued that it may contain a large admixture of pentaquark component [1], which will explain the reversed mass ordering between the $S_{11}(1535)$ and $P_{11}(1440)$. By studying this reaction, one can extract the ηN interaction, for which a possible strong attraction between η and N at low energies may lead to “ η -mesic nuclei” [2, 3]. In general, more and more accurate data from $\pi^-p \rightarrow \eta n$ experiments will provide a challenging testing ground for the low energy theories of hadron interactions, such as chiral perturbation theory, meson-exchange model, etc.

On the process $\pi^-p \rightarrow \eta n$, there have been a few experiments. The data come mainly from the old measurements about thirty years ago [4, 5, 6, 7, 8, 9], which have been reviewed by Clajus and Nefkens [10]. Fortunately, a recent $\pi^-p \rightarrow \eta n$ experiment was performed at BNL using the Crystal Ball spectrometer [11]. The differential cross sections together with total cross section for η production in reaction $\pi^-p \rightarrow \eta n$ have been measured at the incident π beam momenta from threshold to $p_\pi = 747$ MeV/c. The quality of the data was significantly improved compared with the previous measurements. Theoretically, a few typical models have been used to deal with the $\pi^-p \rightarrow \eta n$ reactions [12, 13, 14, 15, 16, 17, 18, 19], such as the coupled-channel model, meson-exchange model, the chiral multi-channel model. As pointed out in ref. [20], the present theory is far from being as accurate as the experiment. Thus, more theoretical studies are needed.

In this work, we introduce an effective chiral Lagrangian to describe the quark-pseudoscalar-meson coupling and study the meson-nucleon scattering in the constituent quark model. This approach has been successfully applied to the study of the meson photoproduction off nucleons [21, 22, 23, 24, 25, 26, 27, 28, 29, 30, 31, 32]. Since the quark-pseudoscalar-meson coupling is invariant under the chiral transformation, some of the low-energy properties of QCD are retained. There are several outstanding features for this model. One is that only a very limited number of parameters will appear in this framework. In particular, only one parameter is need for the resonances to be coupled to the pseudoscalar mesons. This distinguishes from hadronic models where each resonance requires one additional coupling constant as free parameter. The second is that all the resonances can be treated consistently in the quark model. Thus, it has predictive powers when exposed to experimental data, and information about the resonance structures can be extracted.

However, it should be clarified that we restrict the quark-meson interactions in the scattering processes where the mesons are external fields interacting with the constituent quarks of the Isgur-Karl model [33]. Thus, the spin-independent quark confinement potential is described by harmonic oscillator potential. This allows an analytic separation of the intermediate meson excitation matrix elements. In principle, the quark-meson interaction will influence the description of the constituent quark potentials, e.g., modifications to the quark interactions may occur and naive quark model spectrum will be changed. We leave this to be investigated in future development of this approach. The

baryon spectroscopy studied via Goldstone-boson exchanges (GBE) can be found in Ref. [34]. Extended chiral quark model approach combining both one-gluon-exchange (OGE) and GBE potentials has also been investigated in the literature [35, 36].

In this work, we have investigated the $\pi^- p \rightarrow \eta n$ reaction from the η production threshold to the c.m. energy $W \simeq 1.7$ GeV. Our results are in good agreement with the data. We find that $S_{11}(1535)$ dominates the reaction around threshold. The resonances $D_{13}(1520)$ and $S_{11}(1650)$ also play very important roles in the process. The $D_{13}(1520)$ is crucial to give correct shapes of the differential cross sections, although its contributions to the cross section are very small near threshold. The $S_{11}(1650)$ has important destructive interferences with the dominant $S_{11}(1535)$ around $W \lesssim 1.6$ GeV. Above the c.m. energy $W \simeq 1.6$ GeV, the contributions of higher resonances from $n = 2$ shell also appear. The predictions of differential cross sections become worse with the increasing c.m. energy W . The resonance $P_{11}(1710)$ plays an important role, it is crucial to produce an enhancement in the region of $W > 1.6$ GeV as suggested by the data for total cross section, and with which the theoretical predictions are obviously improved if we change the sign of its amplitude. The nucleon pole term contributions turn out to be necessary though a relatively small $g_{\eta NN}$ coupling is favored. The t -channel is negligible in the reactions.

The paper is organized as follows. In the subsequent section, the framework is outlined. Then, the transition amplitudes in the quark model are derived in Sec. III. The resonance contributions are separated out in Sec. IV. We present our calculations and discussions in Sec. V. Finally, a summary is given in Sec. VI.

II. FRAMEWORK

In the chiral quark model, the low energy quark-meson interactions are described by the effective Lagrangian [27, 29]

$$\mathcal{L} = \bar{\psi}[\gamma_\mu(i\partial^\mu + V^\mu + \gamma_5 A^\mu) - m]\psi + \dots, \quad (1)$$

where V^μ and A^μ correspond to vector and axial currents, respectively. They are given by

$$\begin{aligned} V^\mu &= \frac{1}{2}(\xi\partial^\mu\xi^\dagger + \xi^\dagger\partial^\mu\xi), \\ A^\mu &= \frac{1}{2i}(\xi\partial^\mu\xi^\dagger - \xi^\dagger\partial^\mu\xi), \end{aligned} \quad (2)$$

with $\xi = \exp(i\phi_m/f_m)$, where f_m is the meson decay constant. For the SU(3) case, the pseudoscalar-meson octet ϕ_m can be expressed as

$$\phi_m = \begin{pmatrix} \frac{1}{\sqrt{2}}\pi^0 + \frac{1}{\sqrt{6}}\eta & \pi^+ & K^+ \\ \pi^- & -\frac{1}{\sqrt{2}}\pi^0 + \frac{1}{\sqrt{6}}\eta & K^0 \\ K^- & \bar{K}^0 & -\sqrt{\frac{2}{3}}\eta \end{pmatrix}, \quad (3)$$

and the quark field ψ is given by

$$\psi = \begin{pmatrix} \psi(u) \\ \psi(d) \\ \psi(s) \end{pmatrix}. \quad (4)$$

From the leading order of the Lagrangian [see Eq.(1)], we obtain the standard quark-meson pseudovector coupling at tree level

$$H_m = \sum_j \frac{1}{f_m} \bar{\psi}_j \gamma_\mu^j \gamma_5^j \psi_j \partial^\mu \phi_m. \quad (5)$$

where ψ_j represents the j -th quark field in the nucleon.

The η meson production amplitude (see Fig. 1) can be expressed in term of the Mandelstam variables:

$$\mathcal{M} = \mathcal{M}_s + \mathcal{M}_u + \mathcal{M}_t. \quad (6)$$

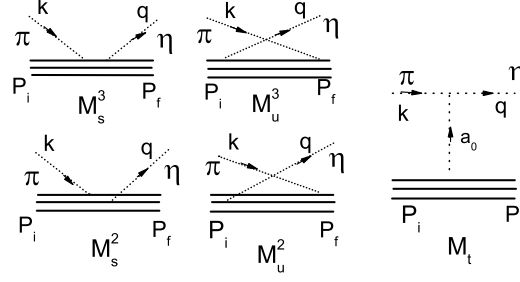


FIG. 1: s - u - and t -channels are considered in this work. M_3^s and M_3^u (M_2^s , M_2^u) correspond to the amplitudes of s - and u -channels for the incoming meson and outgoing meson absorbed and emitted by the same quark (different quarks), respectively.

The s - and u -channel transitions are given by

$$\mathcal{M}_s = \sum_j \langle N_f | H_\eta | N_j \rangle \langle N_j | \frac{1}{E_i + \omega_\pi - E_j} H_\pi | N_i \rangle, \quad (7)$$

$$\mathcal{M}_u = \sum_j \langle N_f | H_\pi \frac{1}{E_i - \omega_\eta - E_j} | N_j \rangle \langle N_j | H_\eta | N_i \rangle, \quad (8)$$

where ω_π and ω_η are the energies of the incoming π -meson and outgoing η -meson, respectively. H_π and H_η are the standard quark-meson couplings at tree level described by Eq.(5). $|N_i\rangle$, $|N_j\rangle$ and $|N_f\rangle$ stand for the initial, intermediate and final states, respectively, and their corresponding energies are E_i , E_j and E_f , which are the eigenvalues of the NRCQM Hamiltonian \hat{H} [33].

Following the procedures developed in refs. [23, 27, 29], one can then express the s and u channel amplitudes by operator expansions. For instance, the s channel can be written as

$$\mathcal{M}_s = \sum_j \langle N_f | H_\eta | N_j \rangle \langle N_j | \sum_n \frac{1}{\omega_\pi^{n+1}} (\hat{H} - E_i)^n H_\pi | N_i \rangle, \quad (9)$$

where n is the harmonic oscillator quantum number. Note that for any operator \mathcal{O} , one has

$$(\hat{H} - E_i) \mathcal{O} | N_i \rangle = [\hat{H}, \mathcal{O}] | N_i \rangle, \quad (10)$$

a systematic expansion of the commutator between the NRCQM Hamiltonian \hat{H} and the vertex coupling H_π and H_η can thus be carried out. Details of this treatment can be found in refs. [23, 27, 29], but we note that in this study only the spin-independent potential in \hat{H} is considered as a feasible leading order calculation.

From PDG [37] we know that the a_0 meson decay is dominated by $\pi\eta$ channel. Thus, we consider a_0 exchange as the dominant contributions to the t -channel transitions. For the $\pi\eta a_0$ coupling, we introduce the following effective Lagrangian

$$\mathcal{L}_{a_0\pi\eta} = g_{a_0\pi\eta} m_\pi \vec{\pi} \vec{a}_0, \quad (11)$$

and for the quark- a_0 coupling, we select a scalar interaction

$$H_{a_0} = \sum_j g_{a_0qq} m_\pi \bar{\psi}_j \psi_j \vec{a}_0, \quad (12)$$

where g_{a_0qq} is the coupling constant for a_0 -quark. According to these interactions, the amplitude of t -channel can be written as

$$\mathcal{M}_t = g_{a_0\pi\eta} m_\pi \langle N_f | H_{a_0} | N_i \rangle \frac{1}{t^2 - m_{a_0}^2}. \quad (13)$$

where m_{a_0} is the mass of a_0 .

In the quark model, the nonrelativistic form of Eq. (5) is written as [27, 29]

$$H_m^{nr} = \sum_j \left\{ \frac{\omega_m}{E_f + M_f} \boldsymbol{\sigma}_j \cdot \mathbf{P}_f + \frac{\omega_m}{E_i + M_i} \boldsymbol{\sigma}_j \cdot \mathbf{P}_i - \boldsymbol{\sigma}_j \cdot \mathbf{q} + \frac{\omega_m}{2\mu_q} \boldsymbol{\sigma}_j \cdot \mathbf{p}_j \right\} \frac{I_j}{g_A} \varphi_m, \quad (14)$$

and the nonrelativistic form of (12) is given by

$$H_{a_0}^{nr} = \sum_j m_\pi (1 + \boldsymbol{\sigma}_j \cdot \mathbf{G}_f \boldsymbol{\sigma}_j \cdot \mathbf{G}_i) I_j \varphi_m, \quad (15)$$

where

$$\mathbf{G}_f = \mathcal{K}_f \mathbf{P}_f + \frac{1}{2m_q} \mathbf{p}_j, \quad (16)$$

$$\mathbf{G}_i = \mathcal{K}_i \mathbf{P}_i + \frac{1}{2m_q} \mathbf{p}_j. \quad (17)$$

with

$$\mathcal{K}_f \equiv \frac{1}{E_f + M_f}, \quad \mathcal{K}_i \equiv \frac{1}{E_i + M_i}. \quad (18)$$

For emitting a meson, we have $\varphi_m = e^{-i\mathbf{q} \cdot \mathbf{r}_j}$, and for absorbing a meson we have $\varphi_m = e^{i\mathbf{q} \cdot \mathbf{r}_j}$. In the above nonrelativistic expansions, vectors \mathbf{r}_j and \mathbf{p}_j are the internal coordinate and momentum for the j -th quark in the nucleon rest frame. ω_m and \mathbf{q} are the energy and three-vector momentum of the meson, respectively. The isospin operator I_j in Eqs. (14) and (15) is expressed as

$$I_j = \begin{cases} a_j^\dagger(d) a_j(u) & \text{for } \pi^- \\ 1 & \text{for } \eta \\ \frac{1}{\sqrt{2}} [a_j^\dagger(u) a_j(u) - a_j^\dagger(d) a_j(d)] & \text{for } a_0 \end{cases}, \quad (19)$$

where $a_j^\dagger(d)$ and $a_j(u)$ are the creation and annihilation operators for the u and d quarks. The axial vector coupling, g_A , relating the hadron spin operator $\boldsymbol{\sigma}$ to the quark spin operator $\boldsymbol{\sigma}_j$ for the j -th quark, is defined as

$$\langle N_f | \sum_j I_j \boldsymbol{\sigma}_j | N_i \rangle \equiv g_A \langle N_f | \boldsymbol{\sigma} | N_i \rangle, \quad (20)$$

which can be explicitly calculated in the NRCQM. For example, for $\pi^- pn$ vertex, one has $g_A^{\pi^-} = 5/3$ and for ηNN , $g_A^\eta = 1$ [27]. The axial vector coupling can then be related to the πNN and ηNN couplings via the Goldberger-Treiman relation [40].

III. AMPLITUDES IN QUARK MODEL

In the calculations, we select the center-mass (c.m.) motion system for the process $\pi N \rightarrow \eta N$. The energies and momenta of the initial meson and nucleon are denoted by (ω_i, \mathbf{k}) and (E_i, \mathbf{P}_i) , while those of the final state meson and nucleon are denoted by (ω_f, \mathbf{q}) and (E_f, \mathbf{P}_f) . Note that $\mathbf{P}_i = -\mathbf{k}$ and $\mathbf{P}_f = -\mathbf{q}$.

A. amplitudes for t -channel

According to Eq. (15), the nonrelativistic scalar coupling of H_{a_0} for t -channel in the c.m. motion system is obtained as

$$H_{a_0}^{nr} = \sum_j m_\pi (1 + \boldsymbol{\sigma}_j \cdot \mathbf{G}'_f \boldsymbol{\sigma}_j \cdot \mathbf{G}'_i) I_j^{a_0} e^{-i(\mathbf{q}-\mathbf{k}) \cdot \mathbf{r}_j}, \quad (21)$$

with

$$\mathbf{G}'_f = -\mathcal{K}_f \mathbf{q} + \frac{1}{2m_q} \mathbf{p}_j, \quad (22)$$

$$\mathbf{G}'_i = -\mathcal{K}_i \mathbf{k} + \frac{1}{2m_q} \mathbf{p}_j. \quad (23)$$

Substituting Eq. (21) into Eq. (13), finally we get the t -channel amplitude at quark level, which is given by

$$\begin{aligned} \mathcal{M}_t = & g_{a_0\pi\eta} m_\pi \frac{1}{t - m_{a_0}^2} \langle N_f | \{ C_0 + C_1 + C_2 \mathbf{k} \cdot \mathbf{q} \\ & + C_3 i \boldsymbol{\sigma}_3 \cdot (\mathbf{q} \times \mathbf{k}) \} 3I_3^{a_0} e^{-(\mathbf{q}-\mathbf{k})^2/6\alpha^2} | N_i \rangle, \end{aligned} \quad (24)$$

where

$$C_0 = m_\pi \left(1 - \frac{1}{2m_q} \frac{1}{2m_q} \frac{\alpha^2}{3} \right) \quad (25)$$

$$C_3 = -m_\pi \left[\mathcal{K}_i \mathcal{K}_f + \frac{1}{6m_q} (\mathcal{K}_i + \mathcal{K}_f) \right], \quad (26)$$

$$C_2 = -m_\pi \left[\mathcal{K}_i \mathcal{K}_f + \frac{1}{6m_q} \left(\mathcal{K}_i + \mathcal{K}_f + \frac{1}{3m_q} \right) \right] \quad (27)$$

$$C_1 = \frac{m_\pi}{6m_q} \left[\left(\frac{1}{6m_q} + \mathcal{K}_f \right) \mathbf{q}^2 + \left(\frac{1}{6m_q} + \mathcal{K}_i \right) \mathbf{k}^2 \right]. \quad (28)$$

To derive the amplitudes for a particular reaction, we have to transform the amplitudes at quark level into the more familiar amplitudes at hadronic level, which is given by

$$\begin{aligned} \mathcal{M}_t = & g_{a_0\pi\eta} g_{a_0NN} \frac{m_\pi}{t - m_{a_0}^2} M_0 \{ g_1 [C_0 + C_1 + C_2 \mathbf{k} \cdot \mathbf{q}] \\ & + g_2 C_3 i \boldsymbol{\sigma} \cdot (\mathbf{q} \times \mathbf{k}) \} e^{-(\mathbf{q}-\mathbf{k})^2/6\alpha^2}, \end{aligned} \quad (29)$$

with $g_1 \equiv \langle N_f | \sum_{j=1}^3 I_j^{a_0} | N_i \rangle$ and $g_2 \equiv \langle N_f | \sum_{j=1}^3 I_j^{a_0} \boldsymbol{\sigma}_j | N_i \rangle$. In this paper, the coupling constant $g_{\pi\eta a_0} g_{a_0 NN}$ is obtained from Refs. [38, 39].

B. amplitudes for s -channel

From Eq. (14), we obtain nonrelativistic couplings of H_π and H_η for the s -channel in the c.m. motion system, which are written as

$$H_\pi = \sum_j \frac{I_j}{g_A^\pi} \boldsymbol{\sigma}_j \cdot \left[\mathbf{A}_\pi e^{i\mathbf{k} \cdot \mathbf{r}_j} + \frac{\omega_\pi}{2m_q} \{ \mathbf{p}_j, e^{i\mathbf{k} \cdot \mathbf{r}_j} \} \right], \quad (30)$$

$$H_\eta = \sum_j \frac{I_j}{g_A^\eta} \boldsymbol{\sigma}_j \cdot \left[\mathbf{A}_\eta e^{-i\mathbf{q} \cdot \mathbf{r}_j} + \frac{\omega_\eta}{2m_q} \{ \mathbf{p}_j, e^{-i\mathbf{q} \cdot \mathbf{r}_j} \} \right], \quad (31)$$

with

$$\mathbf{A}_\pi = - \left(\frac{\omega_\pi}{E_i + M_i} + 1 \right) \mathbf{k}, \quad (32)$$

$$\mathbf{A}_\eta = - \left(\frac{\omega_\eta}{E_f + M_f} + 1 \right) \mathbf{q}. \quad (33)$$

Substituting Eqs. (30) and (31) into Eq.(7), then following the procedures used in refs. [23, 27, 29], we obtain the s -channel amplitude in the harmonic oscillator basis, which is expressed as

$$\mathcal{M}^s = \sum_n (\mathcal{M}_3^s + \mathcal{M}_2^s) e^{-(\mathbf{k}^2 + \mathbf{q}^2)/6\alpha^2}, \quad (34)$$

where α is the oscillator strength, and $e^{-(\mathbf{k}^2+\mathbf{q}^2)/6\alpha^2}$ is a form factor in the harmonic oscillator basis. \mathcal{M}_3^s (\mathcal{M}_2^s) corresponds to the amplitudes for the outgoing meson and incoming meson absorbed and emitted by the same quark (different quarks). They are given by

$$\begin{aligned} \mathcal{M}_3^s = & \langle N_f | \frac{3I_3}{g_A^\pi} \left\{ \boldsymbol{\sigma}_3 \cdot \mathbf{A}_\eta \boldsymbol{\sigma}_3 \cdot \mathbf{A}_\pi \sum_{n=0} \frac{F_s(n)}{n!} \mathcal{X}^n + \left[-\boldsymbol{\sigma}_3 \cdot \mathbf{A}_\eta \frac{\omega_\pi}{3m_q} \boldsymbol{\sigma}_3 \cdot \mathbf{q} - \frac{\omega_\eta}{3m_q} \boldsymbol{\sigma}_3 \cdot \mathbf{k} \boldsymbol{\sigma}_3 \cdot \mathbf{A}_\pi + \frac{\omega_\eta}{m_q} \frac{\omega_\pi}{m_q} \frac{\alpha^2}{3} \right] \right. \\ & \times \sum_{n=1} \frac{F_s(n)}{(n-1)!} \mathcal{X}^{n-1} + \frac{\omega_\eta}{3m_q} \frac{\omega_\pi}{3m_q} \boldsymbol{\sigma}_3 \cdot \mathbf{q} \boldsymbol{\sigma}_3 \cdot \mathbf{k} \sum_{n=2} \frac{F_s(n)}{(n-2)!} \mathcal{X}^{n-2} \left. \right\} | N_i \rangle, \end{aligned} \quad (35)$$

and

$$\begin{aligned} \mathcal{M}_2^s = & \langle N_f | \frac{6I_1}{g_A^\pi} \left\{ \boldsymbol{\sigma}_1 \cdot \mathbf{A}_\eta \boldsymbol{\sigma}_3 \cdot \mathbf{A}_\pi \sum_{n=0} \frac{F_s(n)}{n!} \frac{\mathcal{X}^n}{(-2)^n} + \left[-\boldsymbol{\sigma}_1 \cdot \mathbf{A}_\eta \frac{\omega_\pi}{3m_q} \boldsymbol{\sigma}_3 \cdot \mathbf{q} - \frac{\omega_\eta}{3m_q} \boldsymbol{\sigma}_1 \cdot \mathbf{k} \boldsymbol{\sigma}_3 \cdot \mathbf{A}_\pi + \frac{\omega_\eta}{m_q} \frac{\omega_\pi}{m_q} \frac{\alpha^2}{3} \boldsymbol{\sigma}_1 \cdot \boldsymbol{\sigma}_3 \right] \right. \\ & \times \sum_{n=1} \frac{F_s(n)}{(n-1)!} \frac{\mathcal{X}^{n-1}}{(-2)^n} + \frac{\omega_\eta}{3m_q} \frac{\omega_\pi}{3m_q} \boldsymbol{\sigma}_1 \cdot \mathbf{q} \boldsymbol{\sigma}_3 \cdot \mathbf{k} \sum_{n=2} \frac{F_s(n)}{(n-2)!} \frac{\mathcal{X}^{n-2}}{(-2)^n} \left. \right\} | N_i \rangle, \end{aligned} \quad (36)$$

where $\mathcal{X} \equiv \frac{\mathbf{k} \cdot \mathbf{q}}{3\alpha^2}$. The subscriptions of the spin operator $\boldsymbol{\sigma}$ denote that it either operates on quark 3 or quark 1.

In the Eqs. (35) and (36), the factor $F_s(n)$ is given by expanding the energy propagator in Eq. (7) (and similarly in Eq. (8)) which leads to

$$F_s(n) = \frac{M_n}{P_i \cdot k - nM_n\omega_h} \quad (37)$$

where n is the total excitation quantum number in the harmonic oscillator basis; M_n is the mass of the excited state in the n -th shell, while ω_h is the typical energy of the harmonic oscillator; P_i and k are the four momenta of the initial state nucleons and incoming π^- mesons in the c.m. system. This factor has clear physical meaning that recovers the hadronic level propagators. We will come back to this in the next section.

The above two transitions can be written coherently in terms of a number of g -factors, which will allow us to relate the quark-level amplitudes to those at hadronic level

$$\begin{aligned} \mathcal{M}^s = & \frac{1}{g_A^\pi} \left\{ \mathbf{A}_\eta \cdot \mathbf{A}_\pi \sum_{n=0} [g_{s1} + (-2)^{-n} g_{s2}] \frac{F_s(n)}{n!} \mathcal{X}^n + \left(-\frac{\omega_\pi}{3m_q} \mathbf{A}_\eta \cdot \mathbf{q} - \frac{\omega_\eta}{3m_q} \mathbf{A}_\pi \cdot \mathbf{k} + \frac{\omega_\eta}{m_q} \frac{\omega_\pi}{m_q} \frac{\alpha^2}{3} \right) \right. \\ & \times \sum_{n=1} [g_{s1} + (-2)^{-n} g_{s2}] \frac{F_s(n)}{(n-1)!} \mathcal{X}^{n-1} + \frac{\omega_\eta \omega_\pi}{(3m_q)^2} \mathbf{k} \cdot \mathbf{q} \sum_{n=2} \frac{F_s(n)}{(n-2)!} [g_{s1} + (-2)^{-n} g_{s2}] \mathcal{X}^{n-2} \\ & + i\boldsymbol{\sigma} \cdot (\mathbf{A}_\eta \times \mathbf{A}_\pi) \sum_{n=0} [g_{v1} + (-2)^{-n} g_{v2}] \frac{F_s(n)}{n!} \mathcal{X}^n + \frac{\omega_\eta \omega_\pi}{(3m_q)^2} i\boldsymbol{\sigma} \cdot (\mathbf{q} \times \mathbf{k}) \\ & \times \sum_{n=2} [g_{v1} + (-2)^{-n} g_{v2}] \frac{F_s(n)}{(n-2)!} \mathcal{X}^{n-2} \left. \right\} e^{-(\mathbf{k}^2+\mathbf{q}^2)/6\alpha^2}. \end{aligned} \quad (38)$$

where the g factors are defined as

$$g_{s1} \equiv \langle N_f | \sum_{j=1}^3 I_j | N_i \rangle, \quad (39)$$

$$g_{v1} \equiv \langle N_f | \sum_{j=1}^3 I_j \sigma_{jz} | N_i \rangle, \quad (40)$$

$$g_{s2} \equiv \langle N_f | \sum_{i \neq j} I_j \boldsymbol{\sigma}_i \cdot \boldsymbol{\sigma}_j | N_i \rangle / 3, \quad (41)$$

$$g_{v2} \equiv \langle N_f | \sum_{i \neq j} I_j (\boldsymbol{\sigma}_i \times \boldsymbol{\sigma}_j)_z | N_i \rangle / 2. \quad (42)$$

The numerical values of these g factors can be derived in the $SU(6) \otimes O(3)$ symmetry limit.

C. amplitudes for u -channel

According to Eq. (14), the nonrelativistic expansions of the u -channel meson-nucleon interactions can also be derived

$$H_\pi = \sum_j \frac{I_j}{g_A^\pi} \boldsymbol{\sigma}_j \cdot \left[\mathbf{B}_\pi e^{i\mathbf{k} \cdot \mathbf{r}_j} + \frac{\omega_\pi}{2m_q} \{\mathbf{p}_j, e^{i\mathbf{k} \cdot \mathbf{r}_j}\} \right], \quad (43)$$

$$H_\eta = \sum_j \frac{I_j}{g_A^\eta} \boldsymbol{\sigma}_j \cdot \left[\mathbf{B}_\eta e^{-i\mathbf{q} \cdot \mathbf{r}_j} + \frac{\omega_\eta}{2m_q} \{\mathbf{p}_j, e^{-i\mathbf{q} \cdot \mathbf{r}_j}\} \right], \quad (44)$$

where

$$\mathbf{B}_\pi = -\omega_\pi (\mathcal{K}_f + \mathcal{K}_j) \mathbf{q} - (\omega_\pi \mathcal{K}_j + 1) \mathbf{k}, \quad (45)$$

$$\mathbf{B}_\eta = -\omega_\eta (\mathcal{K}_i + \mathcal{K}_j) \mathbf{k} - (\omega_\eta \mathcal{K}_i + 1) \mathbf{q}, \quad (46)$$

with $\mathcal{K}_j \equiv 1/(E_j + M_j)$.

Following the same procedure in III B, we obtain amplitudes for the outgoing meson and incoming meson absorbed and emitted by the same quark

$$\begin{aligned} \mathcal{M}_3^u = & -\langle N_f | \frac{3I_3}{g_A^\pi} \left\{ \boldsymbol{\sigma}_3 \cdot \mathbf{B}_\pi \boldsymbol{\sigma}_3 \cdot \mathbf{B}_\eta \sum_{n=0} F_u(n) \frac{1}{n!} \mathcal{X}^n + \left[-\boldsymbol{\sigma}_3 \cdot \mathbf{B}_\pi \frac{\omega_\eta}{3m_q} \boldsymbol{\sigma}_3 \cdot \mathbf{k} - \frac{\omega_\pi}{3m_q} \boldsymbol{\sigma}_3 \cdot \mathbf{q} \boldsymbol{\sigma}_3 \cdot \mathbf{B}_\eta + \frac{\omega_\eta}{m_q} \frac{\omega_\pi}{m_q} \frac{\alpha^2}{3} \right] \right. \\ & \times \sum_{n=1} F_u(n) \frac{\mathcal{X}^{n-1}}{(n-1)!} + \frac{\omega_\eta}{3m_q} \frac{\omega_\pi}{3m_q} \boldsymbol{\sigma}_3 \cdot \mathbf{k} \boldsymbol{\sigma}_3 \cdot \mathbf{q} \sum_{n=2} F_u(n) \frac{\mathcal{X}^{n-2}}{(n-2)!} \left. \right\} | N_i \rangle, \end{aligned} \quad (47)$$

and by different quarks

$$\begin{aligned} \mathcal{M}_2^u = & -\langle N_f | \frac{6I_1}{g_A^\pi} \left\{ \boldsymbol{\sigma}_1 \cdot \mathbf{B}_\pi \boldsymbol{\sigma}_3 \cdot \mathbf{B}_\eta \sum_{n=0} \frac{F_u(n)}{n!} \frac{\mathcal{X}^n}{(-2)^n} + \left[-\boldsymbol{\sigma}_1 \cdot \mathbf{B}_\pi \frac{\omega_\eta}{3m_q} \boldsymbol{\sigma}_3 \cdot \mathbf{k} - \frac{\omega_\pi}{3m_q} \boldsymbol{\sigma}_1 \cdot \mathbf{q} \boldsymbol{\sigma}_3 \cdot \mathbf{B}_\eta + \frac{\omega_\eta}{m_q} \frac{\omega_\pi}{m_q} \frac{\alpha^2}{3} \boldsymbol{\sigma}_1 \cdot \boldsymbol{\sigma}_3 \right] \right. \\ & \times \sum_{n=1} \frac{F_u(n)}{(n-1)!} \frac{\mathcal{X}^{n-1}}{(-2)^n} + \frac{\omega_\eta}{3m_q} \frac{\omega_\pi}{3m_q} \boldsymbol{\sigma}_1 \cdot \mathbf{k} \boldsymbol{\sigma}_3 \cdot \mathbf{q} \sum_{n=2} \frac{F_u(n)}{(n-2)!} \frac{\mathcal{X}^{n-2}}{(-2)^n} \left. \right\} | N_i \rangle, \end{aligned} \quad (48)$$

where the factor $F_u(n)$, which can be related to the propagators, is written as

$$F_u(n) = \frac{M_n}{P_i \cdot q + nM_n\omega_h}, \quad (49)$$

where q are the four momenta of the outgoing η mesons in the c.m. system.

The total amplitude for the u -channel is expressed as

$$\begin{aligned} \mathcal{M}^u = & \frac{-1}{g_A^\pi} \left\{ \mathbf{B}_\pi \cdot \mathbf{B}_\eta \sum_{n=0} [g_{s1} + (-2)^{-n} g_{s2}] \frac{F_u(n)}{n!} \mathcal{X}^n + \left(-\frac{\omega_\eta}{3m_q} \mathbf{B}_\pi \cdot \mathbf{k} - \frac{\omega_\pi}{3m_q} \mathbf{B}_\eta \cdot \mathbf{q} + \frac{\omega_\pi}{m_q} \frac{\omega_\eta}{m_q} \frac{\alpha^2}{3} \right) \right. \\ & \times \sum_{n=1} [g_{s1} + (-2)^{-n} g_{s2}] \frac{F_u(n)}{(n-1)!} \mathcal{X}^{n-1} + \frac{\omega_\eta \omega_\pi}{(3m_q)^2} \mathbf{k} \cdot \mathbf{q} \sum_{n=2} \frac{F_u(n)}{(n-2)!} [g_{s1} + (-2)^{-n} g_{s2}] \mathcal{X}^{n-2} \\ & + i\boldsymbol{\sigma} \cdot (\mathbf{B}_\pi \times \mathbf{B}_\eta) \sum_{n=0} [g_{v1} + (-2)^{-n} g_{v2}] \frac{F_u(n)}{n!} \mathcal{X}^n - \frac{\omega_\eta \omega_\pi}{(3m_q)^2} i\boldsymbol{\sigma} \cdot (\mathbf{q} \times \mathbf{k}) \sum_{n=2} [g_{v1} + (-2)^{-n} g_{v2}] \\ & \times \frac{F_u(n)}{(n-2)!} \mathcal{X}^{n-2} + i\boldsymbol{\sigma} \cdot \left[-\frac{\omega_\eta}{3m_q} (\mathbf{B}_\pi \times \mathbf{k}) - \frac{\omega_\pi}{3m_q} (\mathbf{q} \times \mathbf{B}_\eta) \right] \sum_{n=1} [g_{v1} + (-2)^{-n} g_{v2}] \mathcal{X}^{n-1} \frac{F_u(n)}{(n-1)!} \left. \right\} \\ & \times e^{-(\mathbf{k}^2 + \mathbf{q}^2)/6\alpha^2}. \end{aligned} \quad (50)$$

The first terms in Eqs. (35), (36), (47) and (48) come from the correlation between the c.m. motion of the pion meson transition operator and the c.m. motion of η -meson transition operator; the second and the third terms are the correlation among the internal and the c.m. motions of the π^- and η transition operators, and their contributions begin with the $n \geq 1$ excited states in the harmonic oscillator basis. The last two terms in these equations correspond to the correlation of the internal motion between the π^- and η transition operators, and their contributions begin with either $n \geq 1$ or $n \geq 2$ excited states. The higher shell resonance amplitudes are suppressed remarkably by the factors $1/n!$ and $\mathcal{X}^n \equiv (\mathbf{k} \cdot \mathbf{q}/3\alpha^2)^n$, which come from the spacial integral.

IV. SEPARATION OF THE RESONANCE CONTRIBUTIONS

The obtained amplitudes, \mathcal{M}^s and \mathcal{M}^u , involve excited states with the total excitation quantum number n in the harmonic oscillator basis, which are degenerate to each other. To see the contributions of individual resonances, we need to separate out the single resonance excitation amplitudes for each n . In this work we only separate out the resonance excitation amplitudes for the s -channel, and treat the resonances in the u -channel as degenerate to n . This is because the resonances in the u -channel contribute virtually and are generally suppressed by the kinematics.

In the amplitudes for the s - and u -channels, the factors $F_s(n)$ and $F_u(n)$ can be rewritten as

$$F_s(n) = \frac{2M_n}{s - M_n^2}, \quad (51)$$

$$F_u(n) = \frac{-2M_n}{u - M_n^2}, \quad (52)$$

where $s [= (P_i + k)^2]$ and $u [= (P_i - q)^2]$ are the Mandelstam variables. Taking into account the effects of the resonance mass and width, we thus substitute a Breit-Wigner distribution for $F_s(n)$, i.e.

$$F_s(n) \rightarrow F_s(R) = \frac{2M_R}{s - M_R^2 + iM_R\Gamma_R}, \quad (53)$$

where M_R and Γ_R are the resonance mass and width, respectively. The resonance transition amplitudes in the s and u -channels can be generally expressed as

$$\mathcal{M}_R^s = \frac{2M_R}{s - M_R^2 + iM_R\Gamma_R} \mathcal{O}_R e^{-(\mathbf{k}^2 + \mathbf{q}^2)/6\alpha^2}, \quad (54)$$

and

$$\mathcal{M}_n^u = \frac{2M_n}{u - M_n^2} \mathcal{O}_n e^{-(\mathbf{k}^2 + \mathbf{q}^2)/6\alpha^2}, \quad (55)$$

respectively, where \mathcal{O}_R and \mathcal{O}_n are determined by the structure of each resonance and their couplings to the meson and nucleon.

It should be pointed out that the introduction of the Breit-Wigner widths in the s -channel is arbitrary in this framework, where the width effects from intermediate resonances cannot be automatically produced. However, since it allows a separation of individual resonances, the inclusion of resonance widths from the experiments will make an explicit connection between the transition amplitudes and individual resonance contributions. It should also be mentioned that such an analytic advantage will only appear in the NRQCD model where a harmonic oscillator potential is employed.

A. $n=0$ shell resonances

For $n = 0$, only the nucleon pole term contributes to the transition amplitude. Its s -channel amplitude is

$$\mathcal{M}_N^s = \mathcal{O}_N \frac{2M_0}{s - M_0^2} e^{-(\mathbf{k}^2 + \mathbf{q}^2)/6\alpha^2}, \quad (56)$$

with

$$\mathcal{O}_N = [g_{s1} + g_{s2}] \mathbf{A}_\eta \cdot \mathbf{A}_\pi + [g_{v1} + g_{v2}] i\boldsymbol{\sigma} \cdot (\mathbf{A}_\eta \times \mathbf{A}_\pi), \quad (57)$$

where M_0 is the nucleon mass.

B. $n=1$ shell resonances

For $n = 1$, only S - and D -waves contribute in the s -channel. Note that the spin independent amplitude for D -waves is proportional to the Legendre function $P_2^0(\cos\theta)$, and the spin dependent amplitude for D -waves is in proportion

to $\frac{\partial}{\partial\theta}P_2^0(\cos\theta)$. Moreover, the S -wave amplitude is independent of the scattering angle. Thus, the S - and D -wave amplitudes can be separated out easily. They are presented as

$$\mathcal{M}^s(S) = \mathcal{O}_S F_s(R) e^{-(\mathbf{k}^2 + \mathbf{q}^2)/6\alpha^2}, \quad (58)$$

$$\mathcal{M}^s(D) = \mathcal{O}_D F_s(R) e^{-(\mathbf{k}^2 + \mathbf{q}^2)/6\alpha^2}, \quad (59)$$

with

$$\begin{aligned} \mathcal{O}_S = & \left(g_{s1} - \frac{1}{2}g_{s2} \right) \left(|\mathbf{A}_\eta| |\mathbf{A}_\pi| \frac{|\mathbf{k}||\mathbf{q}|}{9\alpha^2} - \frac{\omega_\pi}{3m_q} \mathbf{A}'_\eta \cdot \mathbf{q} \right. \\ & \left. - \frac{\omega_\eta}{3m_q} \mathbf{A}_\pi \cdot \mathbf{k} + \frac{\omega_\eta}{m_q} \frac{\omega_\pi}{m_q} \frac{\alpha^2}{3} \right), \end{aligned} \quad (60)$$

$$\begin{aligned} \mathcal{O}_D = & \left(g_{s1} - \frac{1}{2}g_{s2} \right) |\mathbf{A}_\eta| |\mathbf{A}_\pi| (3\cos^2\theta - 1) \frac{|\mathbf{k}||\mathbf{q}|}{9\alpha^2} \\ & + \left(g_{v1} - \frac{1}{2}g_{v2} \right) i\boldsymbol{\sigma} \cdot (\mathbf{A}_\eta \times \mathbf{A}_\pi) \frac{\mathbf{k} \cdot \mathbf{q}}{3\alpha^2}. \end{aligned} \quad (61)$$

For the S -waves, the possible resonances are $S_{11}(1535)$ ($[\mathbf{70},^2\mathbf{8}]$) and $S_{11}(1650)$ ($[\mathbf{70},^4\mathbf{8}]$); and for the D -waves, the possible resonances are $D_{13}(1520)$ ($[\mathbf{70},^2\mathbf{8}]$), $D_{13}(1700)$ ($[\mathbf{70},^4\mathbf{8}]$) and $D_{15}(1675)$ ($[\mathbf{70},^4\mathbf{8}]$). The separated amplitudes for the S and D -wave can thus be re-written as

$$\mathcal{M}^s(S) = [g_{S_{11}(1535)} + g_{S_{11}(1650)}] \mathcal{M}^s(S), \quad (62)$$

$$\begin{aligned} \mathcal{M}^s(D) = & [g_{D_{13}(1520)} + g_{D_{13}(1700)} + g_{D_{15}(1675)}] \\ & \times \mathcal{M}^s(D), \end{aligned} \quad (63)$$

where the factor g_R ($R = S_{11}(1535)$, etc) represents the resonance transition strengths in the spin-flavor space, and is determined by the matrix elements $\langle N_f | H_\eta | N_j \rangle \langle N_j | H_\pi | N_i \rangle$. Their relative strengths can be explicitly determined by the following relations

$$\frac{g_{S_{11}(1535)}}{g_{S_{11}(1650)}} = \frac{\langle N_f | \boldsymbol{\sigma}_3 | S_{11}(1535) \rangle \langle S_{11}(1535) | I_3 \boldsymbol{\sigma}_3 | N_i \rangle}{\langle N_f | \boldsymbol{\sigma}_3 | S_{11}(1650) \rangle \langle S_{11}(1650) | I_3 \boldsymbol{\sigma}_3 | N_i \rangle}, \quad (64)$$

$$\frac{g_{D_{13}(1520)}}{g_{D_{13}(1700)}} = \frac{\langle N_f | \boldsymbol{\sigma}_3 | D_{13}(1520) \rangle \langle D_{13}(1520) | I_3 \boldsymbol{\sigma}_3 | N_i \rangle}{\langle N_f | \boldsymbol{\sigma}_3 | D_{13}(1700) \rangle \langle D_{13}(1700) | I_3 \boldsymbol{\sigma}_3 | N_i \rangle}, \quad (65)$$

$$\frac{g_{D_{13}(1700)}}{g_{D_{15}(1675)}} = \frac{\langle N_f | \boldsymbol{\sigma}_3 | D_{13}(1700) \rangle \langle D_{13}(1700) | I_3 \boldsymbol{\sigma}_3 | N_i \rangle}{\langle N_f | \boldsymbol{\sigma}_3 | D_{15}(1675) \rangle \langle D_{15}(1675) | I_3 \boldsymbol{\sigma}_3 | N_i \rangle}. \quad (66)$$

The determined values are listed in Tab. I.

Finally, we obtain the partial amplitudes for individual resonances

$$\mathcal{M}^s(S_{11}(1535)) = g_{S_{11}(1535)} \mathcal{M}^s(S), \quad (67)$$

$$\mathcal{M}^s(S_{11}(1650)) = g_{S_{11}(1650)} \mathcal{M}^s(S), \quad (68)$$

$$\mathcal{M}^s(D_{13}(1520)) = g_{D_{13}(1520)} \mathcal{M}^s(D), \quad (69)$$

$$\mathcal{M}^s(D_{13}(1700)) = g_{D_{13}(1700)} \mathcal{M}^s(D), \quad (70)$$

$$\mathcal{M}^s(D_{15}(1675)) = g_{D_{15}(1675)} \mathcal{M}^s(D). \quad (71)$$

C. $n=2$ shell resonances

For $n = 2$, only the P and F -wave are involved in the s -channel. Note that the spin-independent amplitude for the P -wave is in proportion to $P_1^0(\cos\theta)$, and the spin-dependent amplitude for the P -wave is in proportion to $\frac{\partial}{\partial\theta}P_1^0(\cos\theta)$; the spin-independent amplitude for the F -wave is in proportion to $P_3^0(\cos\theta)$, and the spin-dependent amplitude for the F -wave is in proportion to $\frac{\partial}{\partial\theta}P_3^0(\cos\theta)$. Thus, the P - and F -wave amplitudes can be separated out. They are given by

$$\mathcal{M}^s(P) = \mathcal{O}_P F_s(R) e^{-(\mathbf{k}^2 + \mathbf{q}^2)/6\alpha^2}, \quad (72)$$

$$\mathcal{M}^s(F) = \mathcal{O}_F F_s(R) e^{-(\mathbf{k}^2 + \mathbf{q}^2)/6\alpha^2}, \quad (73)$$

with

$$\begin{aligned} \mathcal{O}_P = & \left[\left(g_{s1} + \frac{1}{4}g_{s2} \right) \left(|\mathbf{A}_\eta||\mathbf{A}_\pi| \frac{|\mathbf{k}||\mathbf{q}|}{10\alpha^2} - \frac{\omega_\pi}{3m_q} \mathbf{A}_\eta \cdot \mathbf{q} - \frac{\omega_\eta}{3m_q} \mathbf{A}_\pi \cdot \mathbf{k} + \frac{\omega_\eta}{m_q} \frac{\omega_\pi}{m_q} \frac{\alpha^2}{3} \right) \right. \\ & + \left(g_{s1} + \frac{1}{4}g_{s2} \right) \frac{3\alpha^2\omega_\eta\omega_\pi}{(3m_q)^2} \frac{|\mathbf{k}||\mathbf{q}|}{3\alpha^2} \cos\theta + \left(g_{v1} + \frac{1}{4}g_{v2} \right) \frac{\omega_\eta\omega_\pi}{(3m_q)^2} i\boldsymbol{\sigma} \cdot (\mathbf{q} \times \mathbf{k}) \\ & \left. + \frac{1}{10} \left(g_{v1} + \frac{1}{4}g_{v2} \right) i\boldsymbol{\sigma} \cdot (\mathbf{A}_\eta \times \mathbf{A}_\pi) \left(\frac{|\mathbf{k}||\mathbf{q}|}{3\alpha^2} \right)^2, \right. \end{aligned} \quad (74)$$

$$\begin{aligned} \mathcal{O}_F = & \left(g_{s1} + \frac{1}{4}g_{s2} \right) \frac{1}{2} |\mathbf{A}_\eta||\mathbf{A}_\pi| \left(\cos^3\theta - \frac{3}{5}\cos\theta \right) \left(\frac{|\mathbf{k}||\mathbf{q}|}{3\alpha^2} \right)^2 + \left(g_{v1} + \frac{1}{4}g_{v2} \right) i\boldsymbol{\sigma} \cdot (\mathbf{A}_\eta \times \mathbf{A}_\pi) \\ & \times \frac{1}{2} \left(\cos^2\theta - \frac{1}{5} \right) \left(\frac{|\mathbf{k}||\mathbf{q}|}{3\alpha^2} \right)^2. \end{aligned} \quad (75)$$

For the P -wave, the possible resonances are $P_{11}(1440)$ ($[\mathbf{56},^2\mathbf{8}]$), $P_{13}(1720)$ ($[\mathbf{56},^2\mathbf{8}]$), $P_{11}(1710)$ ($[\mathbf{70},^2\mathbf{8}]$), $P_{13}(1900)$ ($[\mathbf{70},^4\mathbf{8}]$, $[\mathbf{70},^2\mathbf{8}]$), $P_{11}(2100)$ ($[\mathbf{70},^4\mathbf{8}]$); and for the F -wave, the possible resonances are $F_{15}(1680)$ ($[\mathbf{56},^2\mathbf{8}]$), $F_{17}(1990)$ ($[\mathbf{70},^4\mathbf{8}]$) and $F_{15}(2000)$ ($[\mathbf{70},^2\mathbf{8}]$, $[\mathbf{70},^4\mathbf{8}]$). Thus the amplitudes for the P and F -wave can be re-written as

$$\begin{aligned} \mathcal{M}^s(P) = & [g_{P_{11}(1440)} + g_{P_{11}(1710)} + g_{P_{13}(1720)} \\ & + g_{P_{13}(1900)}] \mathcal{M}^s(S), \end{aligned} \quad (76)$$

$$\mathcal{M}^s(F) = [g_{F_{15}(1680)} + g_{F_{15}(2000)}] \mathcal{M}^s(D), \quad (77)$$

with the same method applied in IV B, we can determine the g_R factors in Eqs. (76) and (77). The g and g_R factors given by the quark model are listed in Tab. I. We find that $g_{D_{13}(1700)}$, $g_{P_{13}(1900)}$ and $g_{P_{11}(2100)}$ is about an order of magnitude less than those of other resonances. Thus, the contributions of $D_{13}(1700)$, $P_{13}(1900)$ and $P_{11}(2100)$ are negligible.

The higher resonances (i.e. $n \geq 3$) are treated as degenerate, for they are less important at the energy region near the threshold of the ηN production.

TABLE I: various g and g_R factors in quark model.

factor	value	factor	value	factor	value
g_{s1}	1	$g_{S_{11}(1535)}$	2	g_2	5/3
g_{s2}	2/3	$g_{S_{11}(1650)}$	-1	$g_{P_{11}(1710)}$	180/619
g_{v1}	5/3	$g_{D_{13}(1520)}$	2	$g_{P_{13}(1900)}$	18/619
g_{v2}	0	$g_{D_{13}(1700)}$	-1/10	$g_{P_{11}(2100)}$	-16/619
g_A^π	5/3	$g_{D_{15}(1675)}$	-9/10	$g_{F_{15}(1680)}$	5/3
g_A^η	1	$g_{P_{11}(1440)}$	225/619	$g_{F_{15}(2000)}$	-2/21
g_1	1	$g_{P_{13}(1720)}$	180/619	$g_{F_{17}(1990)}$	-4/7

TABLE II: Breit-Wigner masses M_R (in MeV) and widths Γ_R (in MeV) for the resonances. $n = 1$ and $n = 2$ stand for the degenerate states with quantum number $n = 1$ and $n = 2$ in the u -channel.

resonance	M_R	Γ_R	resonance	M_R	Γ_R
$S_{11}(1535)$	1535	150	$P_{11}(1440)$	1440	300
$S_{11}(1650)$	1655	165	$P_{11}(1710)$	1710	100
$D_{13}(1520)$	1520	115	$P_{13}(1720)$	1720	200
$D_{13}(1700)$	1700	115	$P_{13}(1900)$	1900	500
$D_{15}(1675)$	1675	150	$P_{11}(2100)$	2100	150
n=1	1650	230	$F_{15}(1680)$	1685	130
n=2	1750	300	$F_{15}(2000)$	2000	200
-	-	-	$F_{17}(1990)$	1990	350

V. CALCULATIONS AND ANALYSIS

A. parameters

Since the resonance amplitudes have been obtained, one can calculate the differential cross section with

$$\frac{d\sigma}{d\Omega} = \frac{(E_i + M_i)(E_f + M_f)}{64\pi^2 s} \frac{|\mathbf{q}|}{|\mathbf{k}|} \frac{1}{2} \sum_{\lambda_i, \lambda_f} |\mathcal{M}_{\lambda_f, \lambda_i}|^2, \quad (78)$$

where $\lambda_i = \pm 1/2$ and $\lambda_f = \pm 1/2$ are the helicities of the initial and final state nucleons, respectively.

To take into account the relativistic effects, as done in [26], we introduce the Lorentz boost factor in the spatial part of the amplitudes, which is

$$\mathcal{O}_i(\mathbf{k}, \mathbf{q}) \rightarrow \gamma_k \gamma_q \mathcal{O}_i(\mathbf{k} \gamma_k, \mathbf{q} \gamma_q), \quad (79)$$

where $\gamma_k = M_i/E_i$ and $\gamma_q = M_f/E_f$.

In the calculations, the quark-pseudoscalar-meson couplings are the overall parameters in the s and u -channel transitions. However, they are not totally free ones. They can be related to the hadronic couplings via the Goldberger-Treiman relation [40]:

$$g_{mNN} = \frac{g_A^m M_N}{f_m}, \quad (80)$$

where m denotes the pseudoscalar mesons, π , η , etc; f_m is the meson decay constant defined earlier and g_A^m is the axial vector coupling for the meson.

The πNN coupling $g_{\pi NN}$ is a well-determined number:

$$g_{\pi NN} = 13.48, \quad (81)$$

thus we fix it in our calculations. The ηNN coupling is the only free parameter in the present calculations, and to be determined by the experimental data. This quantity has not been well established in both experiment and theory. Its values extracted from different models are still controversial and possess large uncertainties. By fitting the data (differential cross section) at $W \leq 1524$ MeV, we find that our calculations favor a small ηNN coupling around $g_{\eta NN} = 0.81$, which is comparable with those deduced from fitting the η photo-production [26, 30, 41]. The small ηNN coupling is also predicted in Refs. [42, 43, 44, 45, 46, 47]. In contrast, the ηNN coupling derived here is much smaller than those used/predicted in [48, 49, 50, 51, 52], which are in a range of $g_{\eta NN} = 4 \sim 9$. It should be noted that we do not expect that one parameter fitting can provide an overall description of the experimental data. Therefore, we only consider the data at $W \leq 1524$ MeV as a reasonable constraint on the $g_{\eta NN}$ and calculation results with $W > 1524$ MeV will present as a prediction.

For the $a_0\pi\eta$ and a_0NN couplings we adopt a commonly used value $g_{a_0 NN} g_{a_0 \pi \eta} = 100$ in the calculation [38, 39].

There are other two overall parameters, m_q and α , from the quark model. In the calculation we adopt their standard values in the the quark model,

$$m_q = 330 \text{ MeV}, \quad (82)$$

$$\alpha^2 = 0.16 \text{ GeV}^2. \quad (83)$$

For those s -channel resonances which generally have a broad width, the treatment for their widths to be constants is not appropriate. Thus, we take the final-state-momentum-dependent width [23, 24, 29, 30]:

$$\Gamma(\mathbf{q}) = \Gamma_R \frac{\sqrt{s}}{M_R} \sum_i x_i \left(\frac{|\mathbf{q}_i|}{|\mathbf{q}_i^R|} \right)^{2l+1} \frac{D(\mathbf{q}_i)}{D(\mathbf{q}_i^R)}, \quad (84)$$

where $|\mathbf{q}_i^R| = ((M_R^2 - M_0^2 + m_i^2)/4M_R^2 - m_i^2)^{1/2}$, and $|\mathbf{q}_i| = ((s - M_0^2 + m_i^2)/4s - m_i^2)^{1/2}$; x_i is the branching ratio of the resonance decaying into a meson with mass m_i and a nucleon, and Γ_R is the total decay width of the s -channel resonance with mass M_R . $D(\mathbf{q}) = e^{-\mathbf{q}^2/3\alpha^2}$ is a fission barrier function.

We adopt the PDG values for the resonance masses and widths [37], which are listed in Tab. II. The contributions of u -channel for $n \geq 1$ shells are negligibly small, which are insensitive to the degenerate masses and widths for these shells. In this work, we take $M_1 = 1650$ MeV ($M_2 = 1750$ MeV), $\Gamma_1 = 230$ MeV ($\Gamma_2 = 300$ MeV) for the degenerate mass and width of $n = 1$ ($n = 2$) shell, respectively.

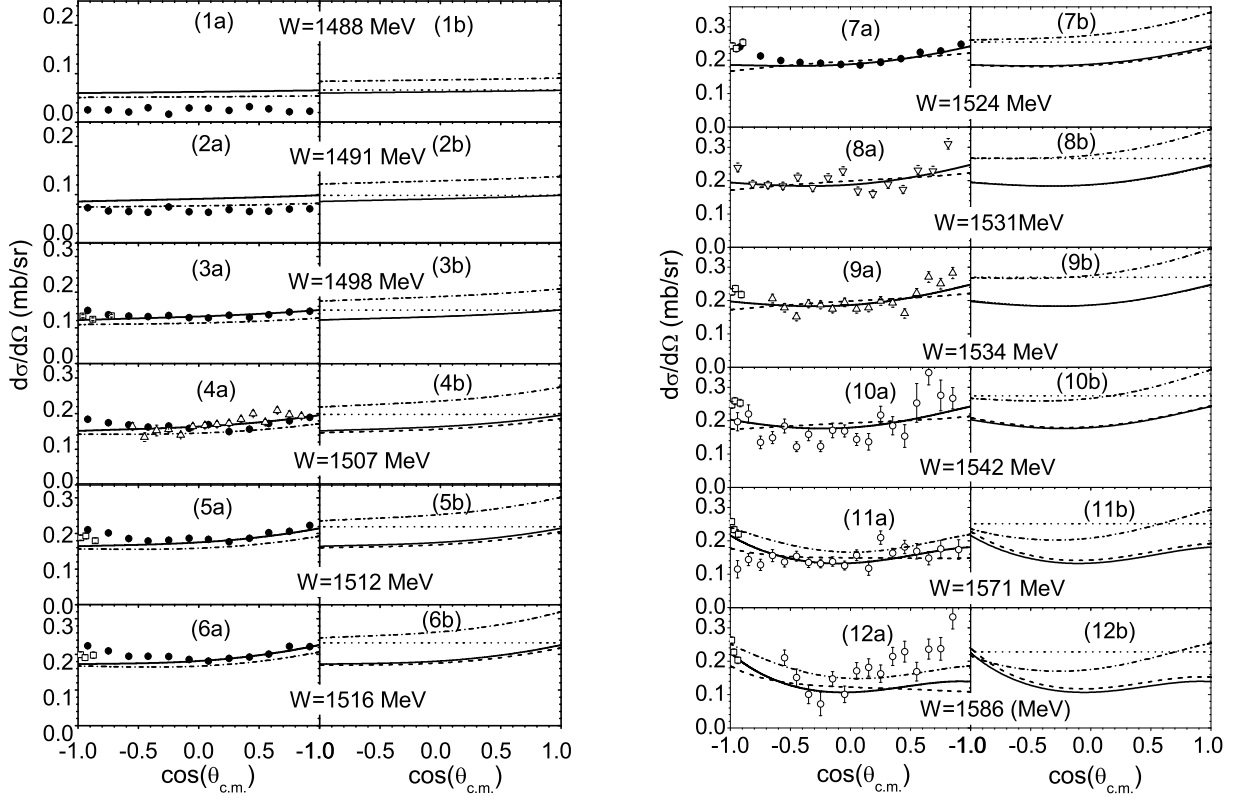


FIG. 2: The differential cross sections at various W . The data are from [4] (open circles), [6] (open up-triangles), [7] (open down-triangles), [9] (open squares), and the recent experiment [11] (solid circles). The solid curves are for the full model differential cross sections. In (1a-12a), the dash-dotted and dashed curves are for the results switched off the contributions from nucleon pole and $D_{13}(1520)$, respectively. In (1b-12b), the dash-dotted and dashed curves correspond to the results without $S_{11}(1650)$ and without t -channel, respectively; the straight lines corresponds to the partial differential cross sections for $S_{11}(1535)$.

B. differential cross section

In Fig. 2, the differential cross sections together with the partial differential cross sections for several individual resonances are shown at different c.m. energies from threshold $W = 1.488$ GeV to $W = 1.586$ GeV. The experimental data [4, 6, 7, 9, 11] are also included for a comparison.

From the figure, we can see that the calculation results agree well with the data as shown by the solid curves. The $S_{11}(1535)$ governs the differential cross sections from the ηN threshold to $W = 1.586$ GeV, as indicated by the straight lines in Fig. 2 (1b-12b).

The $S_{11}(1650)$ has significant destructive interferences with the $S_{11}(1535)$ in the region of $W \leq 1.586$ GeV [see the dash-dotted curves in Fig. 2 (1b-12b)].

If we switch off the $D_{13}(1520)$, as illustrated by the dashed curves in Fig. 2 (7a-12a), we find that the shape of the differential cross sections changes significantly. It shows that the interference between $D_{13}(1520)$ and $S_{11}(1535)$ are crucial to produce the correct shape for the differential cross section around the ηN threshold. This feature is mentioned in [39, 53], and similar feature also appears in photoproduction reactions [30, 41, 42, 54, 55].

The nucleon pole term contributions are visible in the differential cross sections [see the dash-dotted curves Fig. 2 (1a-12a)]. Due to its interference, the differential cross sections are enhanced in the region of $W \lesssim 1.53$ GeV, and suppressed in the region of $W \gtrsim 1.54$ GeV by the nucleon pole.

To see the effects from the t -channel, we also show the differential cross sections without the contributions of it, which are denoted by the dashed curves in Fig. 2 (1b-12b). In the region of $W < 1.586$ GeV, we find that the contributions from t -channel are very small. Basically, its effects on the differential cross sections are negligible in this region.

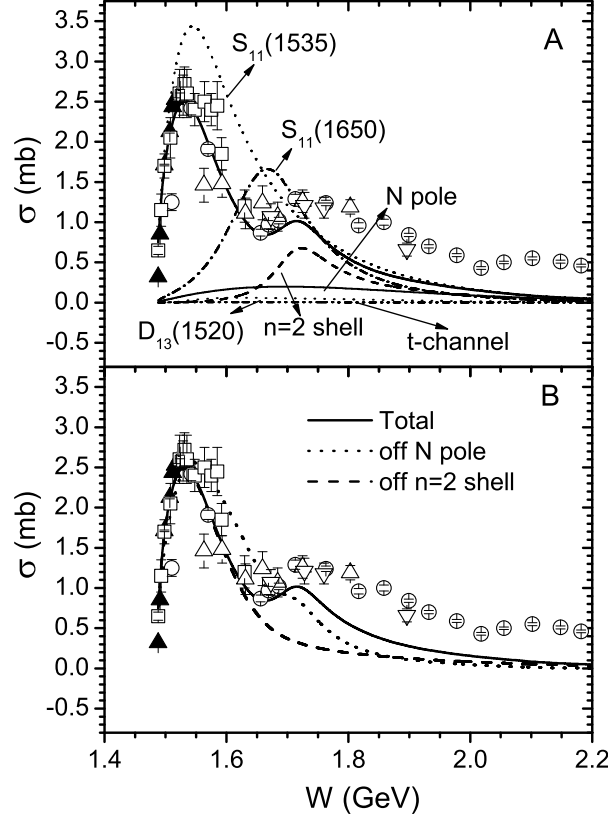


FIG. 3: The cross section as a function of W . The data are from [4] (open circles), [5] (open up-triangles), [8] (open down-triangles), [10] (open squares), and the recent experiment [11] (solid triangles). The solid curves correspond to the full model result. In A, the partial cross sections for $S_{11}(1535)$, $S_{11}(1650)$, $D_{13}(1520)$, $n = 2$ shell and nucleon pole are indicated by different lines and labelled by corresponding text, respectively. In B, the dotted and dashed curves are for the results switched off the contributions from nucleon pole and $n = 2$ shell resonances, respectively.

There are nearly no contributions from $D_{13}(1700)$, $D_{15}(1675)$ and $n = 2$ shell resonances for their large Breit-Wigner masses and /or very small g_R factors. If we switch off their contributions, the changes of the differential cross sections are nearly invisible, thus, we do not show them in Fig. 2.

Above $W = 1.60$ GeV, contributions of the P and F -wave resonances from $n = 2$ shell are present, which will be discussed in Sec. VD.

In brief, in the region of $W \lesssim 1.60$ GeV the resonance $S_{11}(1535)$ governs the process; $D_{13}(1520)$ and $S_{11}(1650)$ play crucial roles in the reactions; the contributions of nucleon pole ($s+u$ -channel) are visible; the contributions from other resonances and t -channel to differential cross sections are rather small.

C. total cross section

The total cross section as a function of the c.m. energy W is plotted in Fig. 3. To see the contributions of each resonance, the partial cross sections of a single resonance are also shown in the same figure. It shows that our theoretical calculations are in a reasonably good agreement with the experimental data up to $W \simeq 1.7$ GeV. At higher energies, although our model gives the correct trend, it underestimates the total cross section. Interestingly, a “second peak” around $W \sim 1.7$ GeV appears in the total cross section, which is also predicted by other models [12, 16, 17].

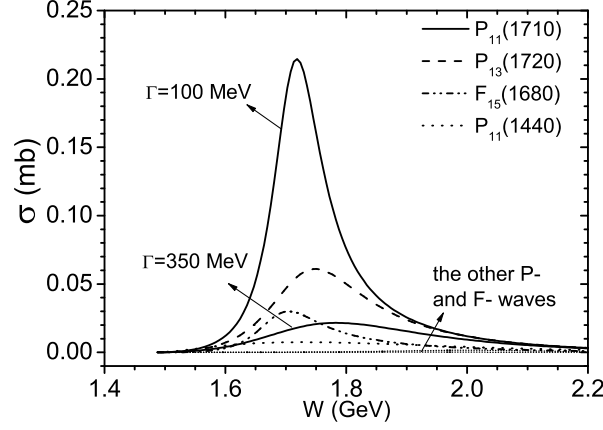


FIG. 4: The partial cross sections for the resonances in $n = 2$ shell are shown. All the Breit-Wigner masses and widths for the resonances are taken from the PDG values. For the $P_{11}(1710)$, the result with a broader width $\Gamma = 350$ MeV is also shown. In the $n = 2$ shell, only $P_{11}(1710)$, $F_{15}(1680)$ and $P_{13}(1720)$ contribute to the cross sections obviously. The other resonances, such as, $P_{13}(1990)$ and $P_{11}(1440)$ nearly have no contributions to the cross sections.

Around the threshold, $W < 1.6$ GeV (i.e., $p_\pi < 0.9$ GeV), we can see that the major contributions to the cross sections are from the $S_{11}(1535)$ and $S_{11}(1650)$. The contributions of the $S_{11}(1535)$ is about an order of magnitude larger than those from the P , D and F wave resonances. In this region, it shows that the exclusive cross section from $S_{11}(1535)$ is even larger than the data. But the destructive interferences from the $S_{11}(1650)$ bring down the cross sections.

For $W > 1.6$ GeV, the contributions of $n = 2$ resonances appear in the reaction. They play important roles around $W = 1.7$ GeV. Without the contributions from $n = 2$ shell, the “second peak” disappears. To know which resonance in $n = 2$ shell contributes to the “second peak”, we should rely on partial wave analysis. It will be discussed in Sec. V D later.

There are nearly no contributions from $D_{13}(1700)$, $D_{15}(1675)$ and $D_{13}(1520)$ in the whole energy region. We should emphasize that, although there are less contributions of $D_{13}(1520)$ to the total cross sections, it plays important roles in the reactions to give a correct shape for the differential cross sections.

From the exclusive cross section of t -channel, we find that the t -channel are negligible to the cross section as shown in Fig. 3-A.

Switching off the the contributions from the nucleon pole terms, we find that the total cross section changes by less than 20% in in the region of $W \lesssim 1.6$ GeV, however it decreases significantly in the region of $W > 1.7$ GeV (see the dash-dot-dotted curve in Fig. 3 B).

A recent analysis of $\pi^- p \rightarrow \eta n$ data suggests the need of the $P_{11}(1710)$ resonance [56, 57]. In the following subsection, we will discuss those higher resonance contributions briefly.

D. higher resonances from $n = 2$ shell

From the analysis in Sections V B, V C, we infer that when the c.m. energy $W < 1.6$ GeV, the data can be accounted for with the resonances of $n \leq 1$. To clarify the role played by the higher resonances, i.e., the P and F -wave states in $n = 2$ shell, we make an analysis of the differential cross sections in the energy region $W > 1.6$ GeV, where the $P_{11}(1710)$, $P_{13}(1720)$ and $F_{15}(1680)$ may become important.

Firstly, to see the contributions from individual resonances [i.e., $P_{11}(1440)$, $P_{11}(1710)$, $P_{13}(1720)$, $P_{13}(1900)$, $P_{11}(2100)$, $F_{15}(1680)$, $F_{15}(2000)$ and $F_{17}(1990)$] we plot their partial cross sections as function of energy in Fig. 4. It shows that the $P_{11}(1710)$ is dominant over other states around $W \sim 1.6 - 1.77$ GeV. Although the contributions of the $P_{13}(1720)$ and $F_{15}(1680)$ are visible, they are about 5 ~ 10 times smaller than the $P_{11}(1710)$. There are nearly no contributions from the $P_{13}(1900)$, $P_{11}(1440)$ and $F_{17}(1990)$ in $n = 2$ in this energy region. We then conclude that to reproduce the “second peak” in Fig. 3 we need the $P_{11}(1710)$, which is consistent with other studies in the literatures [56, 57].

In Fig. 5, the differential cross sections at $W = 1.609, 1.657$ and 1.670 GeV are presented. It shows that without the

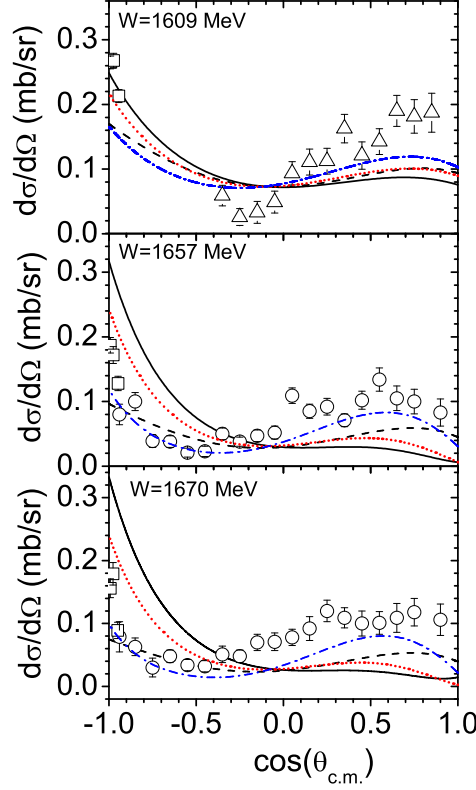


FIG. 5: (Color online) The differential cross sections for $W = 1.609, 1.657$ and 1.670 GeV, respectively (solid curves). Data are obtained from [4] (open circles). The dashed curves are for the prediction without the $n = 2$ shell resonances. The dash-dotted curves are for the case when we reverse the sign of the partial amplitude for $P_{11}(1710)$.

$P_{11}(1710)$, $F_{15}(1680)$ and $P_{13}(1720)$, the changes to the differential cross section are rather significant. We find that the theoretical predictions overestimate the cross sections at backward angles, while underestimate the cross sections at forward angles, compared with the data. Since there are still large uncertainties with the width of the $P_{11}(1710)$ (i.e. $\Gamma = 50 \sim 450$ MeV) [12, 37], we thus adjust it to examine the model predictions. By setting width as $\Gamma = 350$ MeV, we find that the predictions at $W = 1.657$ and 1.670 GeV are improved obviously (see the dotted curves in Fig. 5). It should be noted that with $\Gamma = 350$ MeV for the $P_{11}(1710)$, its partial cross sections decrease significantly, and its contributions becomes comparable with those of $P_{13}(1720)$ and $F_{15}(1680)$ (see Fig. 4). Although the predictions are improved by using a broader width for $P_{11}(1710)$, there still exists a big gap between the theoretical predictions and the data.

Interestingly, the data seem to favor that the contribution from the $P_{11}(1710)$ has a reversed sign as shown by the dash-dotted curves. It also improves the parameter fitting. This could be a signal for the breakdown of the $SU(6) \otimes O(3)$ symmetry within the P -wave states. A similar example is the radial excited $P_{11}(1440)$ of [56, 28] which is lighter than the first orbital excited $S_{11}(1535)$ and suggests the breakdown of the non-relativistic constituent quark model (NRCQM) [33].

It has also been discussed in the literature that the $P_{11}(1710)$ could be a candidate for the $1/2^+$ pentaquark with hidden strangeness [58]. It was shown in ref. [59] that a possible mixture of the $[20, 28]$ within the P -wave states can break down the naive quark model symmetry and make their properties very different from the NRCQM expectations. Our present study certainly does not allow us to conclude the nature of the $P_{11}(1710)$. But the results seem to show that the data favor a strong P -wave contribution with a reversed sign in respect of the $P_{11}(1710)$ around $W \sim 1.7$ GeV, for which the source should be investigated. Polarization observables in this energy region may be sensitive to its interference and a partial wave analysis of data should be pursued.

VI. SUMMARY

We have extended the chiral quark model approach for meson photo-production on nucleon to the study of meson-production in meson-nucleon scatterings. An major advantage of this approach is that the number of free parameters will be greatly reduced in the quark model as the leading order calculation. For the reaction $\pi^- p \rightarrow \eta n$ at low energies, we succeed in accounting for the differential and total cross sections from threshold to the third resonance region.

In this study, we find that the $S_{11}(1535)$ and $S_{11}(1650)$ dominate the reaction in a wide energy region above the threshold. Although contributions from the $D_{13}(1520)$ and nucleon pole terms are relatively small near threshold, they are crucial to produce the correct shape of the differential cross sections via interferences. In particular, the $S_{11}(1650)$ has a destructive interference with the $S_{11}(1535)$ near threshold, and the $D_{13}(1520)$ is crucial to produce the angular distributions. The t -channel contributions are negligible in the reactions. Above the c.m. energy $W \sim 1.6$ GeV, the contributions of higher resonances from $n = 2$ shell also appear. The $P_{11}(1710)$ plays an important role around the c.m. energy $W = 1.7$ GeV, which contributes to the bump around $W = 1.7$ GeV in the total cross section. It turns out that a sign change for the $P_{11}(1710)$ will better account for the data. This could be a sign for the breakdown of the NRCQM and state mixings are needed. It may also be a signal of unconventional configurations inside the $P_{11}(1710)$ for which both improved experimental measurement and theoretical phenomenology are required.

Acknowledgements

This work is supported, in part, by the National Natural Science Foundation of China (Grants 10675131, 10775145), Chinese Academy of Sciences (KJCX3-SYW-N2), the U.K. EPSRC (Grant No. GR/S99433/01), the Post-Doctoral Programme Foundation of China, and K. C. Wong Education Foundation, Hong Kong.

-
- [1] B. C. Liu and B. S. Zou, Phys. Rev. Lett. **96**, 042002 (2006) [arXiv:nucl-th/0503069].
 - [2] Q. Haider and L. C. Liu, Phys. Lett. B **172**, 257 (1986); L. C. Liu and Q. Haider, Phys. Rev. C **34**, 1845 (1986).
 - [3] V. Baru *et al.*, arXiv:nucl-th/0610011.
 - [4] R. M. Brown *et al.*, Nucl. Phys. B **153**, 89 (1979).
 - [5] F. Bulos *et al.*, Phys. Rev. **187**, 1827 (1969).
 - [6] W. Deinet, H. Mueller, D. Schmitt, H. M. Staudenmaier, S. Buniatov, E. Zavattini, Nucl. Phys. B **11**, 495 (1969).
 - [7] J. Feltesse *et al.*, Nucl. Phys. B **93**, 242 (1975).
 - [8] W. B. Richards *et al.*: Phys. Rev. D **1**, 10 (1970).
 - [9] N. C. Debenham *et al.*, Phys. Rev. D **12**, 2545 (1975).
 - [10] M. Clajus and B. M. K. Nefkens, PiN Newslett. **7**, 76 (1992).
 - [11] S. Prakhov *et al.*: Phys. Rev. C **72**, 015203 (2005).
 - [12] G. Penner and U. Mosel, Phys. Rev. C **66**, 055211 (2002) [arXiv:nucl-th/0207066].
 - [13] R. A. Arndt, W. J. Briscoe, T. W. Morrison, I. I. Strakovsky, R. L. Workman and A. B. Gridnev, Phys. Rev. C **72**, 045202 (2005) [arXiv:nucl-th/0507024].
 - [14] R. A. Arndt, W. J. Briscoe, I. I. Strakovsky, R. L. Workman and M. M. Pavan, Phys. Rev. C **69**, 035213 (2004) [arXiv:nucl-th/0311089].
 - [15] A. M. Gasparyan, J. Haidenbauer, C. Hanhart and J. Speth, Phys. Rev. C **68**, 045207 (2003) [arXiv:nucl-th/0307072].
 - [16] M. Batinic, I. Slaus, A. Svarc and B. M. K. Nefkens, Phys. Rev. C **51**, 2310 (1995) [Erratum-ibid. C **57**, 1004 (1998)] [arXiv:nucl-th/9501011].
 - [17] V. Shklyar, G. Penner and U. Mosel, Eur. Phys. J. A **21**, 445 (2004) [arXiv:nucl-th/0403064].
 - [18] T. Feuster and U. Mosel, Phys. Rev. C **58**, 457 (1998) [arXiv:nucl-th/9708051].
 - [19] T. P. Vrana, S. A. Dytman and T. S. H. Lee, Phys. Rept. **328**, 181 (2000) [arXiv:nucl-th/9910012].
 - [20] C. Hanhart, Acta Phys. Slov. **56**, 193 (2005) [arXiv:nucl-th/0511045].
 - [21] T. Abdullah and F. E. Close, Phys. Rev. D **5**, 2332 (1972).
 - [22] F. E. Close and Z. P. Li, Phys. Rev. D **42**, 2194 (1990).
 - [23] Z. P. Li, Phys. Rev. D **48**, 3070 (1993).
 - [24] Z. P. Li, Phys. Rev. D **50**, 5639 (1994).
 - [25] Z. P. Li, Phys. Rev. C **52**, 1648 (1995).
 - [26] Z. P. Li, Phys. Rev. D **52**, 4961 (1995).
 - [27] Z. P. Li, H. X. Ye and M. H. Lu, Phys. Rev. C **56**, 1099 (1997) [arXiv:nucl-th/9706010].
 - [28] Q. Zhao, Phys. Rev. C **64**, 052201(R) (2001).
 - [29] Q. Zhao, J. S. Al-Khalili, Z. P. Li and R. L. Workman, Phys. Rev. C **65**, 065204 (2002) [arXiv:nucl-th/0202067].
 - [30] Q. Zhao, B. Saghai and Z. P. Li, J. Phys. G **28**, 1293 (2002) [arXiv:nucl-th/0011069].

- [31] Q. Zhao, Z. P. Li and C. Bennhold, Phys. Rev. C **58**, 2393 (1998) [arXiv:nucl-th/9806100].
- [32] Q. Zhao, Z. P. Li and C. Bennhold, Phys. Lett. B **436**, 42 (1998) [arXiv:nucl-th/9803015].
- [33] N. Isgur and G. Karl, Phys. Lett. **72B**, 109 (1977); N. Isgur and G. Karl, Phys. Rev. D **18**, 4187 (1978); *ibid* D **19**, 2653 (1979); Erratum **23**, 817 (1981); *ibid* D **20**, 1191 (1979).
- [34] L. Y. Glozman and D. O. Riska, Phys. Rept. **268**, 263 (1996) [arXiv:hep-ph/9505422].
- [35] Z. Y. Zhang, Y. W. Yu, P. N. Shen, L. R. Dai, A. Faessler and U. Straub, Nucl. Phys. A **625**, 59 (1997).
- [36] F. Huang and Z. Y. Zhang, Phys. Rev. C **72**, 024003 (2005) [arXiv:nucl-th/0507025].
- [37] W. M. Yao *et al.*, J. Phys. G **33**, 1 (2006).
- [38] O. Krehl, C. Hanhart, S. Krewald, and J. Speth, Phys. Rev. C **62**, 025207 (2000).
- [39] A. M. Gasparyan, J. Haidenbauer, C. Hanhart, and J. Speth, Phys. Rev. C **68**, 045207 (2003).
- [40] M. L. Goldberger and S. B. Treiman, Phys. Rev. **110**, 1178 (1958).
- [41] Z. P. Li and B. Saghai, Nucl. Phys. A **644**, 345 (1998); B. Saghai and Z. Li, Eur. Phys. J. A **11**, 217 (2001), [nucl-th/0104084]; Proceedings of NSTAR 2002 Workshop on the Physics of Excited Nucleons, Pittsburgh, Pennsylvania, 9-12 Oct 2002, S.A. Dytman and E.S. Swanson (Editors), World Scientific (2003) [nucl-th/0305004].
- [42] L. Tiator, C. Bennhold and S. S. Kamalov, Nucl. Phys. A **580**, 455 (1994) [arXiv:nucl-th/9404013].
- [43] M. Kirchbach and L. Tiator, Nucl. Phys. A **604**, 385 (1996) [arXiv:nucl-th/9601002].
- [44] S. L. Zhu, Phys. Rev. C **61**, 065205 (2000) [arXiv:nucl-th/0002018].
- [45] W. Grein and P. Kroll, Nucl. Phys. A **338**, 332 (1980).
- [46] V. G. J. Stoks and T. A. Rijken, Phys. Rev. C **59**, 3009 (1999) [arXiv:nucl-th/9901028].
- [47] J. Piekarewicz, Phys. Rev. C **48**, 1555 (1993).
- [48] V. Baru, A. M. Gasparyan, J. Haidenbauer, C. Hanhart, A. E. Kudryavtsev, and J. Speth, Phys. Rev. C **67**, 024002 (2003).
- [49] R. Machleidt, K. Holinde, and Ch. Elster Phys. Rep. **149**, 1 (1987).
- [50] R. Machleidt, Adv. Nucl. Phys. **19**, 189 (1989).
- [51] N. F. Nasrallah, Phys. Lett. B **645**, 335 (2007) [arXiv:hep-ph/0512048].
- [52] M.T. Peña, H. Garcilazo, and D.O. Riska, Nucl. Phys. A **683**, 322 (2001).
- [53] R. A. Arndt, W. J. Briscoe, T. W. Morrison, I. I. Strakovsky, and R. L. Workman, Phys. Rev. C **72**, 045202 (2005).
- [54] W. T. Chiang, S. N. Yang, L. Tiator and D. Drechsel, Nucl. Phys. A **700**, 429 (2002) [arXiv:nucl-th/0110034].
- [55] L. Tiator, D. Drechsel, G. Knochlein and C. Bennhold, Phys. Rev. C **60**, 035210 (1999) [arXiv:nucl-th/9902028].
- [56] V. Shklyar, H. Lenske, U. Mosel, nucl-th/0611036.
- [57] S. Ceci, A. Svarc and B. Zauner, Phys. Rev. Lett. **97**, 062002 (2006) [arXiv:hep-ph/0603144].
- [58] R. Jaffe and F. Wilczek, Phys. Rev. Lett. **91**, 232003 (2003) [arXiv:hep-ph/0307341].
- [59] Q. Zhao and F.E. Close, Phys. Rev. D **74**, 094014 (2006).